ASSESSING INTER-SENSOR ALIGNMENT OF DIWATA-2'S HIGH PRECISION TELESCOPE

Kristian R. Monay[1]*, Fritz Rhaem M. Olivar[1], Benjamin Jonah P. Magallon[1], Paul Leonard Atchong C. Hilario[2],
Czar Jakiri S. Sarmiento[1]

[1]Training Center for Applied Geodesy and Photogrammetry, University of the Philippines Diliman
Diliman, Quezon City, Philippines
Email: krmonay@stamina4space.upd.edu.ph

[2]Institute of Environmental Science and Meteorology, University of the Philippines Diliman
Diliman, Quezon City, Philippines

ABSTRACT: Diwata-2's High-Precision Telescope (HPT) is a multispectral optoelectronic payload, functioning in four bands namely, Red (600 nm to 700 nm), Green (500 nm to 630 nm), Blue (340 nm to 500 nm), and near-infrared or NIR (700 nm to 1000 nm). The HPT also boasts a spatial resolution of 4.7 m ground sensing distance (GSD). Due to its multispectral nature and high resolution, the HPT is suitable for damage assessment as well as detecting landscape changes post-disaster. Accurate stacking of the images across bands assures the resulting remote measurements are as precise as possible. However, due to manufacturing errors, strong vibrations during launch, as well as thermoelastic effects while in orbit, the sensors would tend to misalign with respect to each other. These misalignments may badly affect some of the necessary preprocessing steps such as layer stacking and direct georeferencing, which in turn affect the calculation of the final remote sensing products. It then becomes necessary to assess the alignment between charge-coupled device (CCD) sensors of each band in order to perform proper compensations during remote sensing product calculations. In this paper, the homography matrix for each of the HPT CCDs was calculated. Each homography matrix represents the misalignment of each CCD, in terms of rotation and translation, along the x, y, and z axes. In all calculations, the Blue CCD is set as the reference due to its position with respect to the optical axis of the imaging optics. The homography matrix was obtained from common points between images collected using the scale-invariant feature transform (SIFT) algorithm. Testing the calculated matrix against the parameters established by Hartley and Zisserman (2004) shows the occurrence of an affine transformation. The tests also show shearing on x and y, which further confirms the transformation. The calculated average misalignment for the Green CCD along x is 112 µm, variance of 1.11 µm, while the average misalignment along y is 86 µm, variance of 0.74 µm. Meanwhile, the average misalignment for the Red CCD is 11 µm, variance of 0.76 µm, along x, and 217 µm, variance of 0.74 µm, along y. Other observations such as CCD rotation and aspect ratio difference were also noted.

1. INTRODUCTION

1.1 Diwata-2 Introduction and Misalignment Detection

The Diwata-2 is the Philippines' second microsatellite succeeding Diwata-1. It is a 50 cm x 50 cm x 50 cm microsatellite with a weight of 50 kg and has the capability to deploy its solar panel arrays when needed (Gonzales et al, 2020). Launched on October 29, 2018, using the H-IIA F40 rocket from the Tanegashima Space Center, Japan, one of its objectives is to monitor and determine the damages caused by natural disasters (Monay et al, 2018). As such, it is imperative for the satellite to produce high-resolution images. With high spatial resolution images, it would help to accurately spot and measure damages on roads and buildings. This is addressed by the satellite's High Precision Telescope (HPT) which has a ground sampling distance of 4.7 m at nadir at an altitude of 621 km. The HPT has four charge-coupled devices (CCD) representing four bands: blue (340 nm to 500 nm), green (500 nm to 630 nm), red (600 nm to 700 nm), and near-infrared (700 nm to 1000 nm). The image in Figure 1 is a sample acquisition image by the HPT.

The Diwata-2 is currently handled by the Sustained Support for Local Space Technology and Applications Mastery, Innovation, and Advancement program (STAMINA4Space). The STAMINA4Space program is funded by the Philippine government's Department of Science and Technology.

Although captured by the same camera, Figure 1 shows that non-overlapping areas exist within the same mission and capture time. This suggests that there is misalignment between the bands. Upon layer stacking the raw images, Figure 2 further shows the misalignment to the image set captured at the same time. This misalignment may be caused by a lot of factors like satellite jitter, the time delay between captures, payload manufacturing, and other external factors, to be discussed in the next sections.

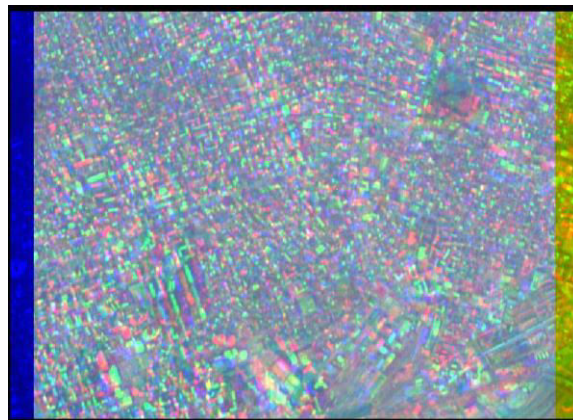Figure 1. Georeferenced Diwata-2 HPT data showing the misalignment of bands.

Figure 2. The stacked raw images from the mission above further showing the misalignment.

1.2 Satellite Launch Effects

During its launch, the satellite is subject to the effects of strong vibrations and high values of acceleration. The Diwata-2 satellite is launched using the H-IIA rocket handled by the Japan Aerospace Exploration Agency (JAXA) and the Mitsubishi Heavy Industries Group (Shoichiro et al, 2003). The payloads attached to the rocket experiences acceleration up to 6.5 G due to the aerodynamic factors and rocket propulsion systems. They also experience vibrations up to 2.5 G during lift-off and the main engine cut-off stage. Shoichiro et al (2003) require all satellites to be transported through the H-IIA rocket to withstand the given conditions. Their paper also requires that the satellite would be subject to high temperatures up to 110°C during launch, and this may cause thermal expansion of the payloads' components.

Thus, there is a possibility that the CCD components of the HPT may have been affected by these launch conditions. Effects such as high acceleration and temperature may change the configuration of these components.

1.3 Manufacturing Factors

For microsatellites, electrical power is an important factor in producing a desirable output. Diwata-2's HPT does not capture using its bands all at the same time. It introduces a time delay between captures to prevent electrical surges to the payload. The payload would snap an image using the blue band first, then green, red, then finally, near-infrared. The time difference between captures causes shifts in the feature locations due to the movement of the satellite.

There is also the factor of machine tolerance. Ideally, the manufacturing of lenses and optomechanical components is exactly as specified in the bill of materials (BOM) and the technical specifications. However, real components contain controlled manufacturing errors (usually specified in technical drawings), in the order of 10-100 micrometers, and tilts in the order of 0.1 degrees. These errors include decentration of the optical components, component tilts, errors in the lens radii of curvature, misalignment of lens surfaces, and irregularities in the lens curvature. These errors result in aberrations in the resulting image such as defocus, distortions, and shifts in the resulting image (Cheng et al, 2007).

1.4 Space Environment Factors

The satellite is exposed to a number of factors while in orbit due to the harsh space environment (Finckenor and de Groh, 2016). Some of these factors include the vacuum of space, which causes outgassing, the presence of atomic oxygen, which causes oxidation on metals and degrades them, and ultraviolet and particulate radiation. These factors affect mostly the material to which the payload is made and may cause the misalignment of small components such as the CCDs.

However, one of the biggest factors that may affect the alignment of components is the large temperature change that the satellite may experience in orbit. Finckenor and de Groh (2016) cautioned on the differences in the coefficients of thermal expansion of the materials in the satellite, which is exemplified on a temperature range of -120°C to +120°C.

1.4 Effects of CCD Misalignment

The misalignment issue is more noticeable when the bands captured at the same time are stacked. Figure 1 shows a ground misalignment of at least 30 meters per band which could accumulate to a maximum of 100 meters. This presents a problem especially in targeting as there may be instances of the target not getting captured by all bands due to this misalignment. Sometimes, the true color stack of the set is needed to determine the area of capture. Misalignment issues introduce more processes, such as georeferencing, for operations to determine the capture area.

This paper's objective is to determine the values of misalignment between bands within the same payload. A misalignment of a few micrometers translates to hundreds of meters in ground distance, which greatly affects the satellite's targeting accuracy and causes georeferencing issues, especially when producing a layer stack image. Determining the values of misalignment between bands would enable direct georeferencing and direct layer stacking, which is useful for capture area determination. It would also determine the areas that are captured within all bands, which is then useful for mission planning purposes and footprint simulation. Finally, the results obtained from this study will be used to monitor the misalignment of the HPT CCDs since launch and determine if it changes significantly during its lifetime.

Kurihara et al (2018) defined a procedure for layer stacking in a similar payload (High Precision Telescope with liquid crystal tunable filter) from the Rising-2 microsatellite. This involved using the scale-invariant feature transform (SIFT) algorithm (Lowe, 2004) to detect key points and using them to estimate the homography matrix between bands. Kurihara et al (2018) also showed the estimated differences between charge-coupled devices (CCD) positions of the HPT has a precision of at least 100 micrometers at the plane perpendicular to the optical axis.

2. TRANSFORMATION MATRIX INVESTIGATION

A homography matrix defines the transformation of one image to another within a single image space, denoted below in Equation 1 as *H* (Malis and Vargas, 2007). It is useful for applying a perspective rectification for planar homographies and, for this study's purposes, retrieving the camera pose for compared images. Since the camera is at a very high altitude of 600 km, it is assumed that the projection plane for images that are close to each other are the same. Equation 1 below also shows that the homography matrix can be inverted for reverse-mapping.

$$\begin{bmatrix} x_2 \\ y_2 \\ 1 \end{bmatrix} = H \begin{bmatrix} x_1 \\ y_1 \\ 1 \end{bmatrix} = \begin{bmatrix} H_{11} & H_{12} & H_{13} \\ H_{21} & H_{22} & H_{23} \\ H_{31} & H_{32} & H_{33} \end{bmatrix} \begin{bmatrix} x_1 \\ y_1 \\ 1 \end{bmatrix} \tag{1}$$

A minimum of four points is needed to define the homography matrix (Malis and Vargas, 2007). This study will use OpenCV's (Bradski, 2000) scale-invariant feature transform (SIFT) algorithm to determine the points present in both images. SIFT is used due to its invariance to scale and rotation changes, which a satellite camera, especially from a microsatellite, is very prone to these changes. SIFT first detects potential key points by finding the extrema of a local neighborhood in its scale and the previous and the next scales made by the Difference of Gaussians (DoG). The collected extrema are organized into low-contrast extrema, edges, and the accepted key points. These accepted key points are then assigned an orientation to make them invariant to rotation, and descriptors are added (Lowe, 2004).

This leads to determining more than the minimum number of points needed for homography matrix estimation, and the least-squares method is used to fit those points into a single homography matrix equation. Images from different

bands were taken at the same timestamp and compared as seen in Figure 3. For this study's purposes, the blue image will be regarded as the reference image for the other bands.
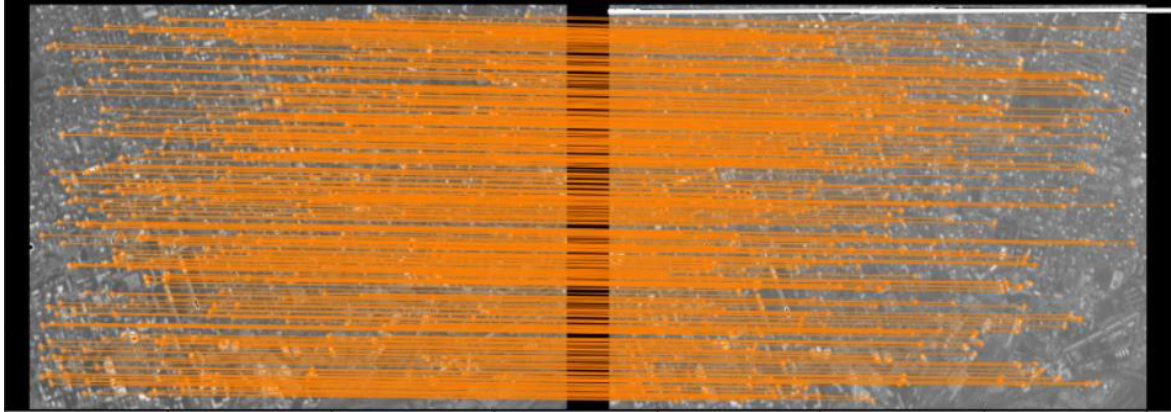

Figure 3. Sample tie point matching between green (left) and blue (right) bands using SIFT.

In this study, only the differences between blue, green, and red bands will be shown, as NIR images do not have enough tie points with the visible bands to produce precise values. The reference frame to be used for this study is a right-handed orthogonal frame with the optical axis as the z-axis, the vertical line on the image as the y-axis, and the x-axis completing the frame. The datasets that will be used for the study are shown below in Table 1. These datasets were chosen to provide variability in terms of capture date and time, and satellite view angles.

Table 1. Missions used in the study

Timestamp (UTC)	Area
2020/05/06 05:47:40.66	Fujian, China
2020/05/06 05:47:44.26	Fujian, China
2020/05/26 05:30:23.62	Chungcheongnam-do, South Korea
2020/10/18 04:35:41.23	Sapporo, Japan

The average homography matrices H are shown below in Tables 2 and 3.

Table 2. Homography matrix for Green to Blue

0.9997746	0.003185752	-15.90823216
-0.00254368	0.984099185	16.6147917
3.91171E-07	-3.05492E-07	1

Table 3. Homography matrix for Red to Blue

0.990862247	0.002379259	1.061118
-0.002395835	0.983594948	34.31767
9.126E-07	-1.48004E-06	1

The homography matrices show a strong similarity to an affine transformation (shown below as Equation 2), with the exception of a very small value on H_{31} and H_{32}, indicating a minimal projective transformation between the bands (Hartley and Zisserman, 2004). An affine transformation has scaling, rotation, translation, and shearing (Hartley and Zisserman, 2004). Points that were transformed using the matrix were reverse mapped using the inverted matrix and yielded their original coordinates.

$$\begin{pmatrix} x' \\ y' \\ 1 \end{pmatrix} = \begin{bmatrix} a_{11} & a_{12} & t_x \\ a_{21} & a_{22} & t_y \\ 0 & 0 & 1 \end{bmatrix} \begin{pmatrix} x \\ y \\ 1 \end{pmatrix} \tag{2}$$

Figure 4 shows a sample result of the transformation. The images used below are from the Chungcheongnam-do, South Korea mission. By inspection, the green CCD is shifted to the left of blue and both the green and red CCDs were shifted below by almost equal distances due to satellite motion.

Figure 4. Misalignment of the green and red CCDs with respect to blue.

Although the obtained homography matrices are closely related to an affine transformation by inspection, tests must still be done to confirm that these matrices have the properties of an affine transformation. Hartley and Zisserman (2004) defined three invariants for affine transformations. The first property states that parallel lines will still be parallel after the transformation. This is present in the dataset as shown in figure 5. After the transformation involving translation and a minimal rotation, the parallel lines are preserved. The images to be used in figures 5 to 7 are from the Chungcheongnam-do, South Korea mission.
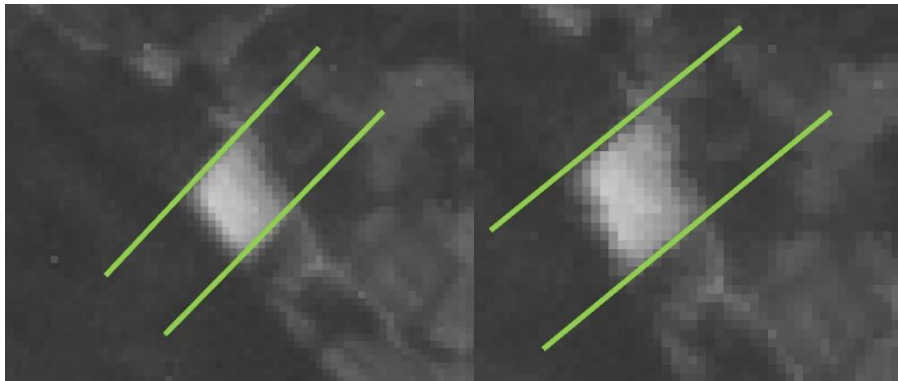

Figure 5. Parallel lines are preserved after transformation. (left, before transformation; right, after transformation)

The second property states that the ratio of parallel line segment lengths must be invariant after transformation. This is shown in figure 6. Two parallel lines are shown below together with their lengths. The ratio of the lengths of the lines before transformation is 0.965913 and after transformation, the ratio is at 0.965969, which has a minimal difference.
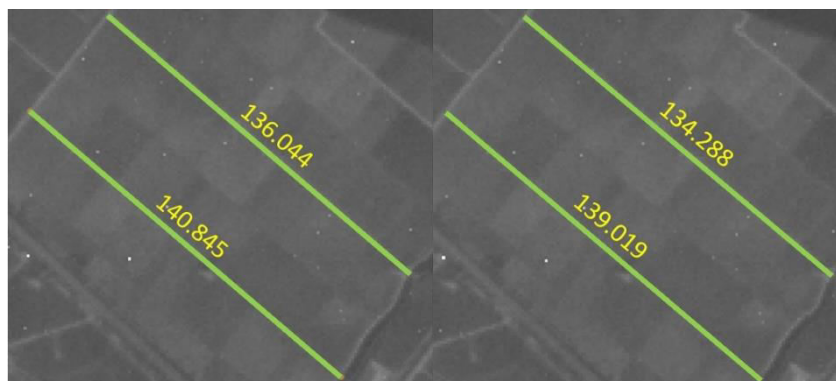

Figure 6. The ratio of the lengths of parallel lines is invariant after transformation. (left, before transformation; right, after transformation)

The final property states that the ratio of areas before and after transformation should still be equal. This is shown in figure 7. The ratio of areas before transformation is 0.654348 and 0.654311 after transformation, which is a minuscule difference.
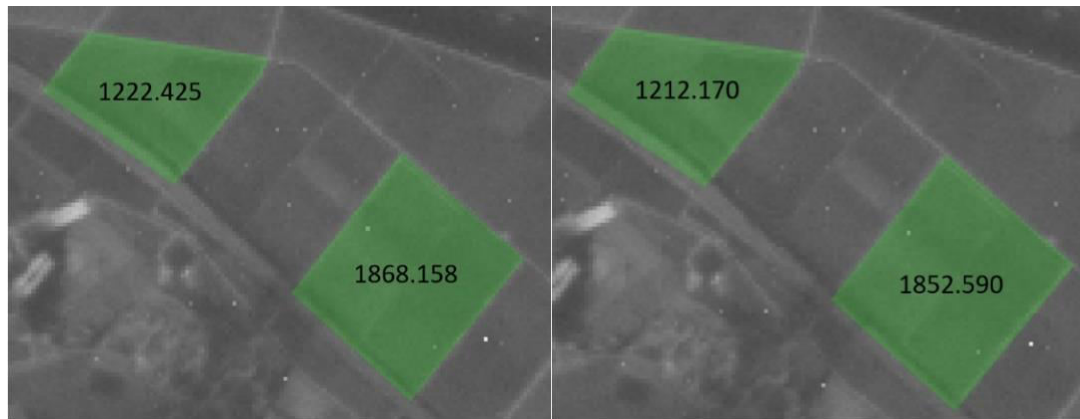
Figure 7. The ratio of areas should be invariant. (left, before transformation; right, after transformation)

By satisfying the three invariant conditions, the obtained matrices define an affine transformation, and the extraction of misalignment values can begin. Since the transformation is affine, the CCDs are perpendicular to the optical axis and the misalignment is caused by a translation and rotation of CCDs relative to the blue CCD.

3. DETERMINATION OF MISALIGNMENT VALUES

To determine the misalignment values, the images are plotted with respect to the blue images, and their positions and orientation were noted. Differences in pixels were measured and converted into real-world measurements using the payload's actual CCD size. Results shall be relative to the blue band. Table 4 shows the coordinates of the corners of the CCDs with respect to blue after the transformation. Table 5 shows the variances on the transformed coordinates. The variances obtained for these corners are small, with maximum variance values of 0.13 for G_x, 0.05 for G_y, 0.18 for R_x, and 0.45 for R_y. This means that there is consistency in the positions of the images per band on all datasets. These small deviations may be attributed to small satellite jitters during capture time. Table 6 shows the actual misalignment values in the x and y axes and their real-world measurements, together with a discovered rotation about the z-axis. Differences in pixel position and orientation were converted into real-world differences using its pixel size (7.4 µm for the HPT).

Table 4. Coordinates of corners per band after transformation

Average	Top Left	Bottom Left	Bottom Right	Top Right
Bx	0	0	691	691
By	0	-503	-503	0
Gx	-15.97704	-14.2809433	676.443515	674.7832375
Gy	-16.5507528	-511.645653	-509.788468	-14.8356293
Rx	1.056388413	2.221397925	687.079535	685.369875
Ry	-34.3932275	-529.452415	-527.38074	-32.5644825

Table 5. SIFT output variances

Variance	Top Left	Bottom Left	Bottom Right	Top Right
Bx	0	0	0	0
By	0	0	0	0
Gx	0.129145882	0.005130047	0.071481005	0.040076212
Gy	0.051131484	0.002328499	0.007394139	0.005308607
Rx	0.031087932	0.078706654	0.180970022	0.034257302
Ry	0.158486838	0.252560188	0.452142405	0.20298706

.

Table 6. Misalignment Report

	Diff *x*	Diff *y*	Rot *z* deg	µm *x*	µm *y*
		2020/05/06 05:47:40.66			
G/B	-15.42683875	-11.63620075	0.256461026	-114.1586068	-86.10788555
R/B	-1.739303575	-29.52456725	0.143095475	-12.87084646	-218.4817976

2020/05/06 05:47:44.26					
G/B	-15.323446	-11.66807625	0.195146897	-113.3935004	-86.34376425
R/B	-1.554053188	-29.3509865	0.1754171	-11.49999359	-217.1973001
2020/05/26 05:30:23.62					
G/B	-15.130179	-11.72161725	0.157118084	-111.9633246	-86.73996765
R/B	-1.4712191	-29.35317675	0.066479312	-10.88702134	-217.213508
2020/10/18 04:35:41.23					
G/B	-15.150767	-11.79460775	0.176344815	-112.1156758	-87.28009735
R/B	-1.51411015	-29.57508575	0.151188209	-11.20441511	-218.8556345
Average					
G/B	-15.25780769	-11.7051255	0.196267705	-112.9077769	-86.6179287
R/B	-1.569671503	-29.45095406	0.134045024	-11.61556912	-217.9370601
Variance					
G/B	0.020208893	0.004800773	0.001851369	1.106638977	0.262890329
R/B	0.01393297	0.013460498	0.002217525	0.76296946	0.737096863

Table 6 shows an x-axis difference of 15.26 and 1.57 pixels shifted to the left for green and red CCDs, respectively. It also shows the y-axis difference of 11.71 and 29.45 pixels shifted downward for the green and red CCDs, respectively. There is also a rotation of about 0.20 and 0.13 degrees for the green and red CCDs, respectively. The misalignment values are converted to real-world measurements, and it was found out that these values are also consistent with the precision determined by Kurihara et al (2018) for the misalignment of the Rising-2 payload.

Since variance values are low especially in the pixel differences, we can assume that the mean values are representative of the misalignment between CCDs. Figure 8 shows the visual misalignment between bands. One can notice the equal distances between the top edges for each band. This may be due to the time delay for the payload to take another image for the other CCDs. This is an operating procedure, as the satellite must save electrical power by capturing areas one CCD at a time. Taking that into account, the average difference between the bands along the y-direction is a multiple of about 16.216 pixels. By using Diwata-2's average speed at 600 km, assuming minimal misalignment at the y-axis, we can also determine the time delay, which is at about 16 ns. Figure 9 shows the effect on the band alignment when the time delay is removed.
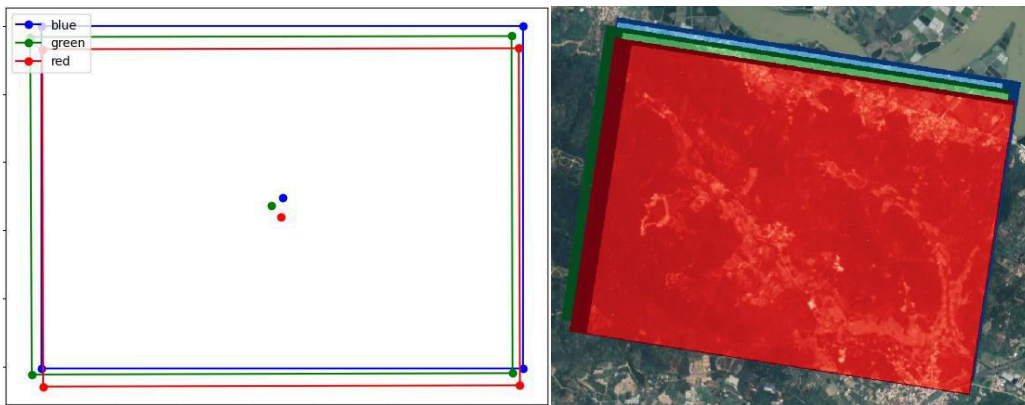

Figure 8. Misalignment between bands. Real-world data shown is the Fujian, China mission.
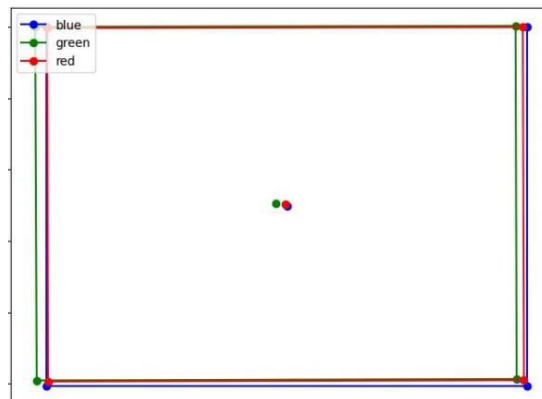

Figure 9. Time delay removed

Figure 9 introduces another misalignment factor between the bands which is the changes to the ratio of CCD length and width. Although the top edges are almost aligned, the bottom edges are not, which suggests that the CCD lengths have changed. Table 7 shows the ratios of the length and width of each band. It is important to note that while the length and width ratios change due to shearing, the property of equal area ratios still holds, as in the case of all affine transformations (Hartley and Zisserman, 2004).

Table 7. Length and Width ratios

	Length	Width
G/B	0.984321	0.999605
R/B	0.984247	0.991129

4. CONCLUSIONS

One of the missions of the Diwata-2 microsatellite is to look at ground objects at a higher resolution through its High Precision Telescope. However, there is misalignment between the payload's charge-coupled devices which hamper direct georeferencing and layer stacking. This misalignment produces a ground error of at least 30 meters, even with the minuscule distances between CCDs within the payload. This paper investigated the transformation matrices among the bands and found out that there is an affine relationship and proved it using the properties of affine transformation as defined by Hartley and Zisserman (2004). For measuring the misalignment, the blue CCD is chosen as the reference due to camera geometry. There is also the advantage of measuring misalignment by pixels to reduce the effect of missions with a high capture angle.

The investigation of the homography matrix determined that the CCDs were aligned about the optical axis and their misalignment can be expressed by translation, rotation, and shearing. It was found out that there is a misalignment of at least 15 pixels or 113 µm in the x-axis for the green CCD which is a lot compared to the 1-pixel misalignment of the red CCD. It was also found out that there is a minimal rotation of about 11 minutes for the green CCD and 8 minutes for the red CCD about the optical axis. Finally, there is the effect of shearing, changing the length and width ratios by a small amount, making the blue CCD larger compared to green and red. The small variance values obtained indicate that the misalignment values were more or less the same throughout all datasets used. The obtained values were also consistent with the payload machine precision of at least 100 micrometers as defined by Kurihara et al (2018).

The determination of misalignment values can be integrated into the operations and initial image processing of Diwata-2 data to lessen the work needed for pre-processing. Although the misalignment values were obtained for the green and red CCDs, there is still the misalignment of the near-infrared CCD, where it was more difficult to investigate as the SIFT algorithm could not accurately find similar points as near-infrared images differ vastly from visible images. Future investigation is required to find a better algorithm that could find correct points between the near-infrared and visible bands. There is also the need to accurately determine the time delay between captures per band to get the actual misalignment for the y-axis, but for the purposes of image pre-processing, the collected values should suffice for now.

5. REFERENCES

Bradski, G., 2000. The OpenCV library. Dr. Dobb's Journal of Software Tools.

Cheng, C. C., Lin, T. Y., and Chen, R. H., 2007. A study on the optomechanical tolerance model for lens assembly. Proc. SPIE 6665, New Developments in Optomechanics, 66650H. https://doi.org/10.1117/12.732241

Finckenor, M., de Groh, K., 2016. A researcher's guide to International Space Station, Space Environmental Effects. NASA ISS Program Science Office. Print.

Gonzalez, A., Labrador, J. L., Mitchao, D., Talampas, M. C., Marciano, J., and Sakamoto, Y., 2020. Diwata-2: Earth observation microsatellite with a compact bus system electronically tunable multi-spectral imager and amateur radio communications capability, in Small Satellite Conference (2020), SSC20-WKII-03.

Hartley, R., and Zisserman, A., 2004. Multiple view geometry in computer vision (2nd ed.). Cambridge: Cambridge University Press. doi:10.1017/CBO9780511811685

Kurihara, J., Takahashi, Y., Sakamoto, Y., Kuwahara, T., and Yoshida, K., 2018. HPT: A high spatial resolution multispectral sensor for microsatellite remote sensing. Sensors (Switzerland), 18(2), [619]. https://doi.org/10.3390/s18020619

Lowe, D. G., 2004. Distinctive image features from scale-invariant keypoints. International Journal of Computer Vision 60, 91–110. https://doi.org/10.1023/B:VISI.0000029664.99615.94

Malis, E., and Vargas, M., 2007. Deeper understanding of the homography decomposition for vision-based control. [Research Report] RR-6303, INRIA., pp.90. ffinria-00174036v3

Monay, K., Olivar, F. R., Magallon, B. J., and Tupas, M. E., 2019. Diwata-2 targeting assessment and attitude error determination using a quaternion-based transformation system. Int. Arch. Photogramm. Remote Sens. Spatial Inf. Sci., XLII-4/W19, 305–311, https://doi.org/10.5194/isprs-archives-XLII-4-W19-305-2019.

Shoichiro, A., Abe, N., Andoh, K., and Fleeter, R., 2003. Launching small satellites on the H-IIA rocket. Proceedings of the Small Satellite Conference, Current Ways to Get to Orbit, SSC03-II-4. https://digitalcommons.usu.edu/smallsat/2003/All2003/12/.